A Progressive Damage Modelling of Glass/Epoxy Cylindrical Structure Subjected to Low-Velocity Impact

Mahrez Ait Mohammed, Mostapha Tarfaoui

Version of Record: https://www.sciencedirect.com/science/article/pii/S1350630722000103
Manuscript_8473818e38cc308c2e1152d82b52fbfc

A Progressive Damage Modelling of Glass/Epoxy Cylindrical Structure Subjected to Low-Velocity Impact

Mahrez Ait Mohammed [1], Mostapha Tarfaoui [1]

[1] ENSTA Bretagne, IRDL - UMR CNRS 6027, 29806 Brest Cedex 9, France

*Corresponding author: mahrez.ait@ensta-bretagne.org
*Corresponding author: mostapha.tarfaoui@ensta-bretagne.fr

Abstract

Due to the harshness and unpredictability of the tidal site environment, the damage induced by an accidental impact should be considered in the certification of composite cylindrical structures intended to be used in the design of the composite MJM tidal turbine concept. The first part of this paper deals with the effect of different failure criteria based on quadratic stress functions on the low-velocity impact response of thick filament wound glass/epoxy cylindrical structures. A user-defined material model (VUMAT) applied to three-dimensional solid elements was implemented into the finite element software Abaqus-Explicit to explore the effect of failure criteria on the predicted dynamic response with intralaminar damage. The investigated failure criteria include the two-dimensional Hashin criteria presented by Hashin in 1973 and extended to the three-dimensional case by including analytically the out-of-plane stress terms (criteria denoted "*Hashin 3D*"), the three-dimensional Hashin criteria described by Hashin in 1980 (criteria denoted "*Hashin 3D 1980*"), the Puck matrix transverse criterion coupled to Hashin criteria (criteria denoted "*Hashin-Puck*") and Chang-Chang criteria (criteria denoted "*Chang & Chang 1987*"). The intralaminar damage model includes damage onset based on quadratic failure criteria, damage evolution, and element deletion from the solid mesh. FEA analyses are carried out with different low-level impact energies. The numerical results show different impact responses as well as the damage characteristics particularly the matrix cracking through the thickness. In the second part the bilinear cohesive zone model (CZM) is employed for modelling the interlaminar damage. The combination of the intralaminar damage model with the interlaminar model is applied using an uncoupled methodology. By comparison with the experimental force-time curves, interface properties used in the cohesive model have been estimated numerically using a reverse methodology and a baseline FEA model. The modelling approach has proven to be capable of reproducing

experimental results with good accuracy. The modelling outcomes and predicted damage are therefore intended to be applied in the design loop and development of the MJM tidal turbine prototype where thick filament wound glass/epoxy cylinders are subjected to low-velocity stones impact.

Keywords: Composite cylinder, impact, dynamic response, progressive damage, delamination.

1. Introduction

Fibre reinforced matrix composites have been widely introduced in the design of marine structures due to their high specific strength and stiffness to density ratios as well as their excellent corrosion resistance. Glass fibre reinforced polymer (GFRP) and carbon fibre reinforced polymer (CFRP) are the most commonly used for marine applications [1]. Thick filament wound glass epoxy cylinders are particularly attractive for such application and are intended to be used in the design loop of the MJM ducted turbine prototype [2] (Fig. 1). Due to the tidal site environment, the turbine is expected to be subjected to impact loads which result in progressive damage and may cause a significant strength and stiffness reduction [3].To fully explore the capabilities of thick filament wound cylinders, it is crucial to investigate with acceptable accuracy the type of failure and its location under dynamic loads. Thorough knowledge of the nature of the damage is necessary to enhance the design efficiency which requires damage tolerance and reliable estimation of the residual lifetime. However, the development of FEA (finite element analysis) modelling techniques combined with advanced material models that describe the damage location and growth based on appropriate failure theory are of great interest to fully master the design loop of complex structures operating in a harsh environment.

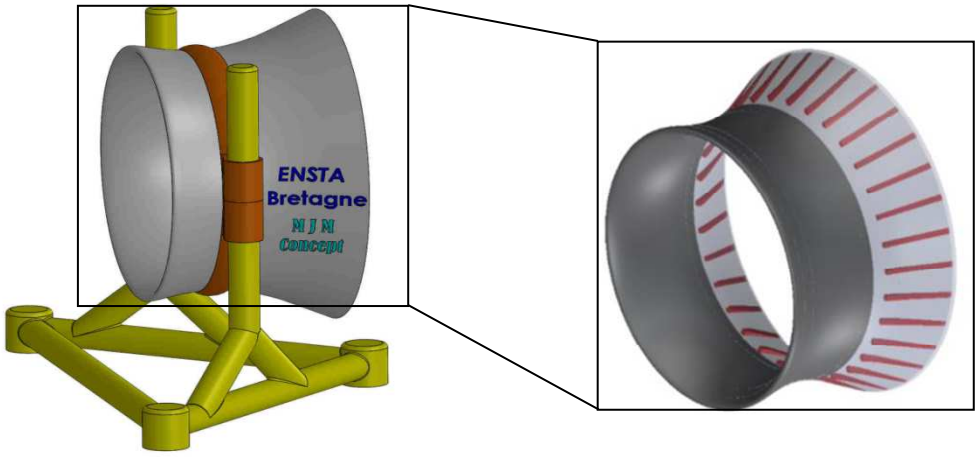

Fig. 1: Inlet cylindrical duct of the MJM tidal turbine and ribs reinforcement at the outlet zone [2]

Damage models have been presented in the literature in recent years dealing with the application of the continuum damage mechanics (CDM) originally introduced by Kachanov [4] and well explained by Lemaitre and Chaboche [5], Maire and Chaboche [6] and more recently by Ladevèze et al. [7] for the failure prediction of composite materials. Research works [8] [9] have investigated a numerical approach based on the CDM which combines

failure criteria for the damage onset, damage variables for the irreversible damage progression and fracture mechanics for the final failure. The results have shown that the application of the CDM can describe very efficiently the damage mechanism in composite subjected to low-velocity impact loads. However other damage models [10] [11] based on plasticity approach combined with failure criteria have been applied for composites that exhibits ductile behaviour under impact loads such as Graphite/PEEK and other thermoplastic composites. Regardless of the numerical approach, the failure theory of composite under impact load is mainly described by damage modes including fibres breakage, matrix cracking, delamination and the interaction between these modes [12].

Many research works published in the literature devoted to the impact modelling of composite cylindrical shapes have considered for the majority an in-plane stress effect only [13] [14] [15]. Krishnamurthy et al. [13] determined the impact response for both a cylindrical shell panel and a full cylinder employing both analytical method and FEA. A parametric study was carried out in the FEA using the Choi-Chang damage model to analyse the effect of varying the controlling model parameters such as impactor mass, velocity and curvature of the cylindrical shell on the impact response and the induced damage. In the analytical method, the deflection as a function of time at the point of impact was obtained using a numerical procedure based on the Fourier series and incorporating the non-linear Hertz's contact law which enables consideration of local indentation produced by the impactor on the cylindrical shell surface. As a result, the authors have shown that force-time curves and the extent of damage obtained for the cylindrical shell panel are very different from that for the full cylindrical shell and the damage suffered by the cylindrical shell panel is significantly higher than that of the full cylindrical shell. Khalili et al. [14] have performed quasi-static and dynamic FEA investigation on composite shell structures and composite cylindrical shells using different side-to-thickness ratios assuming a linear elastic behaviour and in plane effect. The dynamic response of different geometries including plate, curved shell laminate, thick shell cylinder and thin shell cylinder was simulated numerically using both rigid and deformable impactor mesh. The authors conclude that in the FEA models with a large degree of freedoms the explicit solver give more realistic results but more CPU time is required. The authors recommend explicit solvers for solving wave oriented models such as impact problems. Hyeon [15] analysed the transient response and damage of a composite laminated cylinder subjected to foreign object impact with consideration of the change in stiffness. The shear deformation theory of a doubly curved shell and Von Karman's large deflection theory

as well as a strain–displacement relation including initial strain terms to consider the stiffness change induced by cylinder stress due to internal pressure were used to develop a geometrically nonlinear finite-element program.

Tarfaoui et al. [16] [17] carried out quasi-static and dynamic analysis on thick filament wounded glass-epoxy cylindrical structure with transversely isotropic plies using Abaqus. The authors developed a numerical impact model implemented into Abaqus based on material property degradation to predict the progressive failure induced by an accidental impact. Once failure in an element is detected, the material property corresponding to that particular failure mode is reduced depending on the material degradation model. However, delaminations were not considered and no distinction is made between damage initiation and propagation in the numerical model.

The purpose of this paper is to compare the effect of different three-dimensional failure criteria including the two-dimensional Hashin and Rotem criteria published in 1973 [18] but extended to the three-dimensional case by including analytically the out-of-plane terms with a quadratic interaction between failure modes (criteria denoted "*Hashin 3D"*), the three-dimensional criteria such described by Hashin in 1980 [19] (criteria denoted "*Hashin 3D 1980"*), Chang & Chang criteria [20] (criteria denoted "*Chang & Chang 1987"*) and finally the Puck transverse criteria [21] coupled with the three-dimensional Hashin criteria [19] (criteria denoted "*Hashin-Puck"*) on the prediction of the intralaminar damage behaviour of thick filament wound glass/epoxy tubular structures under low-velocity impact. The ply failure model comparing the effect of different failure criteria is performed by developing a user-defined material subroutine (VUMAT) implemented in Abaqus/ Explicit. The intralaminar damage model includes damage onset based on quadratic failure criteria where each criterion is associated to a specific failure mode, linear damage evolution law, and element deletion from the solid mesh when the element is fully damaged. Initially, the dynamic response of the E-glass epoxy cylindrical structure is carried out considering only the intralaminar damage model where four failure criteria have been compared under different impact energies. Once the effect of intralaminar failure criteria is compared, the interlaminar damage is included in the model by employing the bilinear cohesive model (CZM) well described by Alfano et al. [22] and available in Abaqus/Explicit. The combination of the intralaminar damage model with the delamination model is based on an uncoupled methodology. By comparison with the experimental force-time curves, interface properties used in the cohesive model have been estimated numerically using a reverse methodology and

a baseline FEA model. The modelling approach has proven to be capable of reproducing experimental results with acceptable accuracy. The damage modelling outcomes are therefore intended to be applied in the design loop and development of the MJM tidal turbine prototype where thick filament wound glass/epoxy cylinders are subjected to low-velocity stones impact.

2. Constitutive Model

2.1. Intralaminar Damage Model

In the orthotropic case and without taking into account the damage occurrence, the behaviour law of orthotropic composite laminates is described by its initial matrix of rigidity (C_{ij}) written as follow:

$$\begin{Bmatrix}\sigma_{11}\\ \sigma_{22}\\ \sigma_{33}\\ \sigma_{12}\\ \sigma_{23}\\ \sigma_{31}\end{Bmatrix} = \begin{bmatrix}C_{11} & C_{12} & C_{13} & 0 & 0 & 0\\ C_{12} & C_{22} & C_{23} & 0 & 0 & 0\\ C_{13} & C_{23} & C_{33} & 0 & 0 & 0\\ 0 & 0 & 0 & G_{12} & 0 & 0\\ 0 & 0 & 0 & 0 & G_{23} & 0\\ 0 & 0 & 0 & 0 & 0 & G_{31}\end{bmatrix} \begin{Bmatrix}\varepsilon_{11}\\ \varepsilon_{22}\\ \varepsilon_{33}\\ 2\varepsilon_{12}\\ 2\varepsilon_{23}\\ 2\varepsilon_{31}\end{Bmatrix} \tag{1}$$

The elastic stiffness terms (C_{ij}) are defined as:

$$C_{11} = E_{11}(1-\nu_{23}\nu_{32})\Gamma \tag{1.2}$$

$$C_{22} = E_{22}(1-\nu_{13}\nu_{31})\Gamma \tag{1.3}$$

$$C_{33} = E_{33}(1-\nu_{12}\nu_{21})\Gamma \tag{1.4}$$

$$C_{12} = E_{11}(\nu_{21}+\nu_{31}\nu_{23})\Gamma \tag{1.5}$$

$$C_{23} = E_{22}(\nu_{32}+\nu_{12}\nu_{31})\Gamma \tag{1.6}$$

$$C_{13} = E_{11}(\nu_{31}+\nu_{21}\nu_{32})\Gamma \tag{1.7}$$

$$\Gamma = 1/(1-\nu_{12}\nu_{21}-\nu_{23}\nu_{32}-\nu_{31}\nu_{13}-2\nu_{21}\nu_{32}\nu_{13}) \tag{1.8}$$

Once the damage initiation criterion is satisfied, the response of the material which describes the stiffness degradation is defined by the following relation:

$$\begin{Bmatrix}\sigma_{11}\\ \sigma_{22}\\ \sigma_{33}\\ \sigma_{13}\\ \sigma_{23}\\ \sigma_{12}\end{Bmatrix} = \begin{bmatrix}dC_{11} & dC_{12} & dC_{13} & 0 & 0 & 0\\ dC_{12} & dC_{22} & C_{23} & 0 & 0 & 0\\ dC_{13} & dC_{23} & dC_{33} & 0 & 0 & 0\\ 0 & 0 & 0 & dG_{13} & 0 & 0\\ 0 & 0 & 0 & 0 & dG_{23} & 0\\ 0 & 0 & 0 & 0 & 0 & dG_{12}\end{bmatrix} \begin{Bmatrix}\varepsilon_{11}\\ \varepsilon_{22}\\ \varepsilon_{33}\\ 2\varepsilon_{13}\\ 2\varepsilon_{23}\\ 2\varepsilon_{12}\end{Bmatrix} \tag{2}$$

The damaged stiffness terms (dC_{ij}) are written as [23]:

$$dC_{11} = (1 - d_f)C_{11} \quad (2.1)$$

$$dC_{22} = (1 - d_f)(1 - d_m)C_{22} \quad (2.2)$$

$$dC_{33} = (1 - d_f)(1 - d_m)C_{33} \quad (2.3)$$

$$dC_{12} = (1 - d_f)(1 - d_m)C_{12} \quad (2.4)$$

$$dC_{23} = (1 - d_f)(1 - d_m)C_{23} \quad (2.5)$$

$$dC_{13} = (1 - d_f)(1 - d_m)C_{13} \quad (2.6)$$

$$dG_{12} = (1 - d_f)(1 - s_{mT}d_{mT})(1 - s_{mC}d_{mC})G_{12} \quad (2.7)$$

$$dG_{23} = (1 - d_f)(1 - s_{mT}d_{mT})(1 - s_{mC}d_{mC})G_{23} \quad (2.8)$$

$$dG_{31} = (1 - d_f)(1 - s_{mT}d_{mT})(1 - s_{mC}d_{mC})G_{31} \quad (2.9)$$

d_f and d_m are the global fibre and matrix damage variables respectively and defined as:

$$d_f = 1 - (1 - df_T)(1 - df_C) \quad (3)$$

$$d_m = 1 - (1 - dm_T)(1 - dm_C) \quad (4)$$

The superscripts T and C in the damage variables (d_{fT}, d_{fC}, d_{mT} et d_{mC}) denote the tension and compression modes respectively. The factors s_{mT} and s_{mC} in the definition of the shear terms dG_{ij} are introduced to control the reduction of shear stiffness caused by matrix tensile and compressive failure respectively as requested in [24].

2.2. Failure Criteria

Failure criteria of the unidirectional composite are commonly expressed as stress polynomial function linked to a damage mode and were essentially developed for two-dimensional cases in orthotropic materials. Paris [25] presented a review of existing failure criteria developed for fibrous composite materials. However, none of these existing criteria consider the third direction through the thickness. In total, four three-dimensional failure criteria have been implemented separately by developing a user-defined material subroutine (VUMAT) linked to Abaqus software.

In the polynomial function of criteria, σ_{ij} are the components of the stress tensor, X_T and X_C denote tensile and compressive strength in the longitudinal direction, Y_T and Y_C denote tensile and compressive strength in the transverse direction, S_{ij} denote the shear strength in the three different planes.

2.2.1. Hashin and Rotem 2D criteria (1973) extended to the 3D case

The two-dimensional Hashin and Rotem failure criteria [18] is extended to the three-dimensional case (denoted *"Hashin 3D"*) by adding the out-of-plane stress components and keeping a quadratic interaction between the failure modes.

- *Fibre tension and compression:*

$$F_{ft} = \left(\frac{\sigma_{11}}{X_T}\right)^2 + \alpha\left(\frac{\sigma_{12}}{S_{12}}\right)^2 + \beta\left(\frac{\sigma_{13}}{S_{13}}\right)^2 \quad (5)$$

The coefficients α and β regulate the contribution of the shear stress σ_{12} and σ_{13} respectively to the fibre tensile mode and were set to equal one.

$$F_{fc} = \left(\frac{\sigma_{11}}{X_C}\right)^2 \quad (6)$$

- *Matrix tension and compression:*

$$F_{mt} = \left(\frac{\sigma_{22}+\sigma_{33}}{Y_T}\right)^2 + \left(\frac{\sigma_{12}}{S_{12}}\right)^2 + \left(\frac{\sigma_{23}}{S_{23}}\right)^2 \quad (7)$$

$$F_{mc} = \left(\frac{\sigma_{22}+\sigma_{33}}{Y_C}\right)^2 + \left(\frac{\sigma_{12}}{S_{12}}\right)^2 + \left(\frac{\sigma_{23}}{S_{23}}\right)^2 \quad (8)$$

2.2.2. Chang and Chang criteria

Chang and Chang criteria [20] (denoted *"Chang & Chang 1987"*) have been used by Meo et al. [26] to simulate the low-velocity impact on aircraft sandwich panel.

- *Fibre tension and compression:*

$$F_{ft} = \left(\frac{\sigma_{11}}{X_T}\right) + \left(\frac{\sigma_{12}}{S_{12}}\right)^2 + \left(\frac{\sigma_{13}}{S_{13}}\right)^2 \quad (9)$$

$$F_{fc} = \left(\frac{\sigma_{11}}{X_C}\right) + \left(\frac{\sigma_{12}}{S_{12}}\right)^2 + \left(\frac{\sigma_{13}}{S_{13}}\right)^2 \quad (10)$$

- *Matrix tension and compression:*

$$F_{mt} = \left(\frac{\sigma_{22}+\sigma_{33}}{Y_T}\right)^2 + \left(\frac{\sigma_{12}}{S_{12}}\right)^2 + \left(\frac{\sigma_{13}}{S_{13}}\right)^2 + \left(\frac{\sigma_{23}}{S_{23}}\right)^2 \quad (11)$$

$$F_{mc} = \left(\frac{\sigma_{22}+\sigma_{33}}{Y_C}\right)^2 \left[\left(\frac{Y_C}{2S_{12}}\right)^2 - 1\right] \left(\frac{\sigma_{22}+\sigma_{33}}{Y_C}\right)^2 + \bar{\tau}\left(\frac{\sigma_{13}}{S_{13}}\right)^2 + \left(\frac{\sigma_{13}}{S_{13}}\right)^2 + \left(\frac{\sigma_{23}}{S_{23}}\right)^2 \quad (12)$$

The coefficient $\bar{\tau}$ regulates the contribution of the shear stress σ_{13} to the matrix compression mode and was set to equal one.

2.2.3. Hashin 3D (1980)

In 1980 Hashin [19] proposed three-dimensional failure criteria for unidirectional fibre composites under cyclic stress (denoted *"Hashin 3D (1980)"*). The proposed criteria present quadratic stress polynomial function expressed in terms of the transversely isotropic invariants of the cyclic stress.

- *Fibre tension and compression:*

$$F_{ft} = \left(\frac{\sigma_{11}}{X_T}\right)^2 + \left(\frac{\sigma_{12}}{S_{12}}\right)^2 + \left(\frac{\sigma_{13}}{S_{13}}\right)^2 \quad (13)$$

$$F_{fc} = \left(\frac{\sigma_{11}}{X_C}\right)^2 \quad (14)$$

- *Matrix tension and compression:*

$$F_{mt} = \left(\frac{\sigma_{22}+\sigma_{33}}{Y_T}\right)^2 + \frac{{\sigma_{23}}^2-\sigma_{22}\sigma_{33}}{{S_{23}}^2} + \left(\frac{\sigma_{12}}{S_{12}}\right)^2 + \left(\frac{\sigma_{13}}{S_{13}}\right)^2 \quad (15)$$

$$F_{mc} = \frac{1}{Y_C}\left(\left(\frac{Y_c}{2S_{23}}\right)^2 - 1\right)(\sigma_{22}+\sigma_{33}) + \frac{(\sigma_{22}+\sigma_{33})^2}{4{S_{23}}^2} + \frac{{\sigma_{23}}^2-\sigma_{22}\sigma_{33}}{{S_{23}}^2} + \left(\frac{\sigma_{12}}{S_{12}}\right)^2 + \left(\frac{\sigma_{13}}{S_{13}}\right)^2 \quad (16)$$

2.2.4. Hashin 3D (1980) coupled to Puck criteria

Compared to Hashin and Chang failure criteria, the theory proposed by Puck [21] considers a fracture plane oriented by a shear angle θ due to transverse compression failure mode. This angle is approximatively 53° for unidirectional composite [27]. The criteria denoted *"Hashin-Puck"* is similar to *"Hashin 3D (1980)"* criteria for the fibre tension, fibre compression, and matrix tension modes except for the matrix transverse compression mode where the Puck theory is considered.

- *Matrix compression ("Hashin-Puck" criteria):*

$$F_{mc} = \left(\frac{\sigma_t^n}{S_{23}^A+\mu_t^n\sigma_n^n}\right)^2 + \left(\frac{\sigma_l^n}{S_{12}+\mu_l^n\sigma_n^n}\right)^2 \quad (17)$$

Where:

$$\sigma_t^n = -\sigma_{22}cos\theta sin\theta + \sigma_{33}cos\theta sin\theta + 2\sigma_{23}(2cos\theta^2 - 1) \quad (17.1)$$

$$\sigma_n^n = \sigma_{22}cos\theta^2 + \sigma_{33}sin\theta^2 + 2\sigma_{23}cos\theta sin\theta \quad (17.2)$$

$$\sigma_l^n = \sigma_{12}cos\theta + \sigma_{13}sin\theta \quad (17.3)$$

$$S_{23}^A = \frac{Y_c}{2}\left(\frac{1-sin\varphi}{cos\varphi}\right) \;\&\; \varphi = 2\theta - 90° \quad (17.4)$$

$$\mu_t^n = tan\,\varphi \quad (17.5)$$

$$\frac{\mu_t^n}{S_{23}^A} = \frac{\mu_l^n}{S_{12}} \quad (17.6)$$

In the above equations, n is the normal direction, t and l are the tangential directions of the transverse plane fracture. S_{23}^{A} is the transverse shear strength in the transverse fracture plane determined by the transverse compressive strength Yc and the material friction angle φ. μ_t^n and μ_t^n are friction coefficients based on the Mohr failure theory [28].

2.3. Damage Evolution

The evolution of the damage can be defined through a linear, exponential, or other softening law. In this study, a bilinear model is considered and the strain rate effect is neglected. When the damage initiation criterion is satisfied, the damage variable (d_i) linked to each failure mode (i) is given by equation (18) [29]. This damage variable varies from 0 corresponding to undamaged material and reaches 1 when the material is fully damaged.

$$d_i = \frac{\delta_{i,eq}^{f}\left(\delta_{i,eq} - \delta_{i,eq}^{0}\right)}{\delta_{i,eq}\left(\delta_{i,eq}^{f} - \delta_{i,eq}^{0}\right)} \qquad \delta_{i,eq}^{0} \le \delta_{i,eq} \le \delta_{i,eq}^{f} \tag{18}$$

The variables $\delta_{i,eq}^{0}$,$\delta_{i,eq}$, $\delta_{i,eq}^{f}$ represent the initial displacement, equivalent displacement and failure displacement respectively. When the point material is fully damaged ($d_i = 1$) the failure displacement variable is computed from the following equation:

$$\delta_{i,eq}^{f} = \frac{2G_i}{\sigma_{i,eq}^{0}} + \delta_{i,eq}^{0} \tag{19}$$

Where G_i is the fracture energy of each failure mode which controls the shaded area of the softening curve shown in Fig. 2.

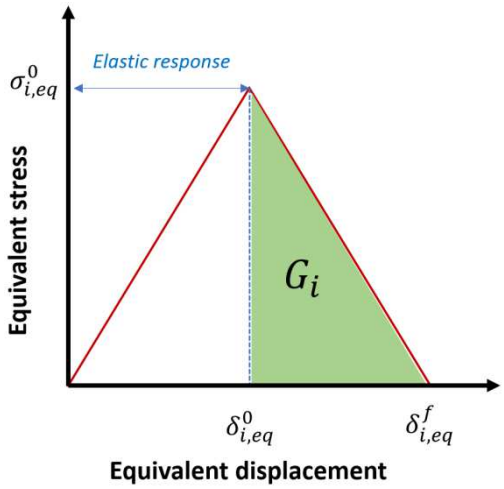

Fig. 2: Intralaminar bilinear law showing the stiffness degradation

The initial equivalent stress ($\sigma^0_{i,eq}$) and the initial equivalent displacement ($\delta^0_{i,eq}$) at which the considered damage initiation criterion (F_i) is satisfied are calculated as:

$$\sigma^0_{i,eq} = \sigma_{i,eq}/\sqrt{F_i} \tag{20}$$

$$\delta^0_{i,eq} = \delta_{i,eq}/\sqrt{F_i} \tag{21}$$

$\sigma_{i,eq}$ and $\delta_{i,eq}$ are equivalent stress and equivalent displacement respectively for each failure mode and are computed as presented in reference [30] (see Table 1).

Table 1: Equivalent displacement and equivalent stress as computed in the linear softening law

Failure mode	Equivalent displacement ($\delta_{i,eq}$)	Equivalent stress ($\sigma_{i,eq}$)
Fibre tension $(\sigma_{11} \geq 0)$	$L_c\sqrt{(\varepsilon_{11})^2 + (\varepsilon_{12})^2 + (\varepsilon_{31})^2}$	$L_c[\sigma_{11}\varepsilon_{11} + \sigma_{12}\varepsilon_{12} + \sigma_{31}\varepsilon_{31}]/\delta_{1,eq}$
Fibre compression $(\sigma_{11} < 0)$	$L_c\sqrt{\left(-\varepsilon_{11} - \frac{\langle\varepsilon_{33}\rangle.E_{33}}{E_{11}}\right)^2}$	$L_c\left[E_{11}\left(-\varepsilon_{11} - \frac{\langle\varepsilon_{33}\rangle.E_{33}}{E_{11}}\right)\right]/\delta_{2,eq}$
Matrix tension $(\sigma_{22} + \sigma_{33} \geq 0)$	$L_c\sqrt{(\varepsilon_{22})^2 + (\varepsilon_{12})^2 + (\varepsilon_{23})^2}$	$L_c[(\sigma_{22}\varepsilon_{22} + \sigma_{12}\varepsilon_{12} + \sigma_{23}\varepsilon_{23})]/\delta_{3,eq}$
Matrix compression $(\sigma_{22} + \sigma_{33} < 0)$	$L_c\sqrt{\left(-\varepsilon_{22} - \frac{\langle\varepsilon_{33}\rangle.E_{33}}{E_{22}}\right)^2 + (\varepsilon_{12})^2}$	$L_c\left[E_{22}\left(-\varepsilon_{22} - \frac{\langle\varepsilon_{33}\rangle.E_{33}}{E_{22}}\right) + \sigma_{12}\varepsilon_{12}\right]/\delta_{4,eq}$

The symbol $\langle\varepsilon_{33}\rangle$ employed in the fibre and matrix compression softening modes is the Mcauley bracket operator:

$$\langle\varepsilon_{33}\rangle = \frac{\varepsilon_{33} + |\varepsilon_{33}|}{2} \tag{22}$$

To reduce the strain localization problem, the concept of characteristic length (L_c) initially proposed by Bažant et al. [31] is applied. The introduction of L_c controls the damage process with a proper description of strain softening. The theory is well explained by Bažant et al. [32] and Pijaudier-Cabot et al. [33]. In the current softening model, we assume that L_c of material point is associated to the element size and equal the cubic root of the solid element volume. However, L_c led to minimize the mesh dependency of the numerical model but does not entirely eradicate the strain-softening problem.

3. Low-velocity Impact of E-Glass/Epoxy Composite Cylinder

3.1. Materials, Geometry and Experimental Procedure

The experimental test on E-glass/epoxy composite cylinders was performed by Gning et al. [34] [35] to study the dynamic response of cylindrical structures of $[\pm 55]_{10}$ stacking sequence. The impacted samples were manufactured using the filament winding process. E-glass fibres were impregnated with a low viscosity epoxy resin. The resin is an LY556 pre-polymer, HY905 hardener and DY061 accelerator from Vantico supplier. The cylinders were cured at 125°C for 7 hours. The measured fibre volume fraction and the porosity were determined as 62% and 6% respectively [34]. The cylinders have an internal diameter of 55mm and a wall thickness of 6.5mm. The adopted notations and coordinates are shown in Fig. 3.

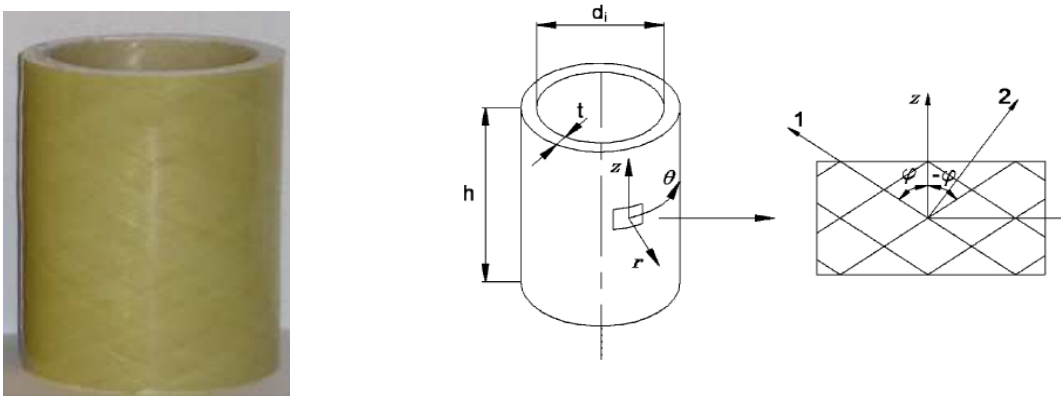

(a) E-glass/epoxy sample *(b) Cylinder coordinates system*

Fig. 3: Sample and geometry

The drop weight impact test was performed by Gning et al. [34] [35] on samples of 110 mm length. The samples, placed in a semi-cylindrical cradle, were impacted using a drop weight device with a hemispherical steel impactor of 50 mm nose diameter. The impactor has a density of 7800 kg/m3, an elasticity modulus of 210 GPa and a Poisson's ratio of 0.3. The impactor was equipped with a piezoelectric accelerometer (Endevco 22556-1) fixed in the tip near the contact point approximately 10 mm from the point of contact with the target. The impact has a normal incidence and occurs at the mid-length of the cylinder. An anti-rebound device was used to allow only a single impact during the experimental test. The impact energy was varied by increasing the drop height to allow the impactor to reach a velocity up to 8 m/s corresponding to the maximum impact energy of 50 J. Fig. 4 shows the test setup employed in

the experimental investigation. Materials properties including elastic and strength constants are taken from [17] and listed in Table 2.

Table 2**: Material property**

Property	**Value**
Density, ρ (kg/m^3)	1960
Longitudinal stiffness, E_{11} (MPa)	49500
Transverse stiffness, E_{22} (MPa)	15900
Out-of-plane stiffness, E_{33} (MPa)	15900
Poisson's ratio, ν_{12}	0.26
Poisson's ratio, ν_{13}	0.26
Poisson's ratio, ν_{23}	0.34
Shear moduli, G_{12} (MPa)	5600
Shear moduli, G_{13} (MPa)	5600
Shear moduli, G_{23} (MPa)	5000
Longitudinal tensile strength, X_t (MPa)	1470
Longitudinal compressive strength, X_c (MPa)	888
Transverse tensile strength, Y_t (MPa)	66
Transverse compressive strength, Y_c (MPa)	99
Out-of-plane tensile strength, Z_t (MPa)	66
Out-of-plane tensile strength, Z_c (MPa)	99
Shear strength, $S_{12} = S_{13} = S_{23}$ (MPa)	66

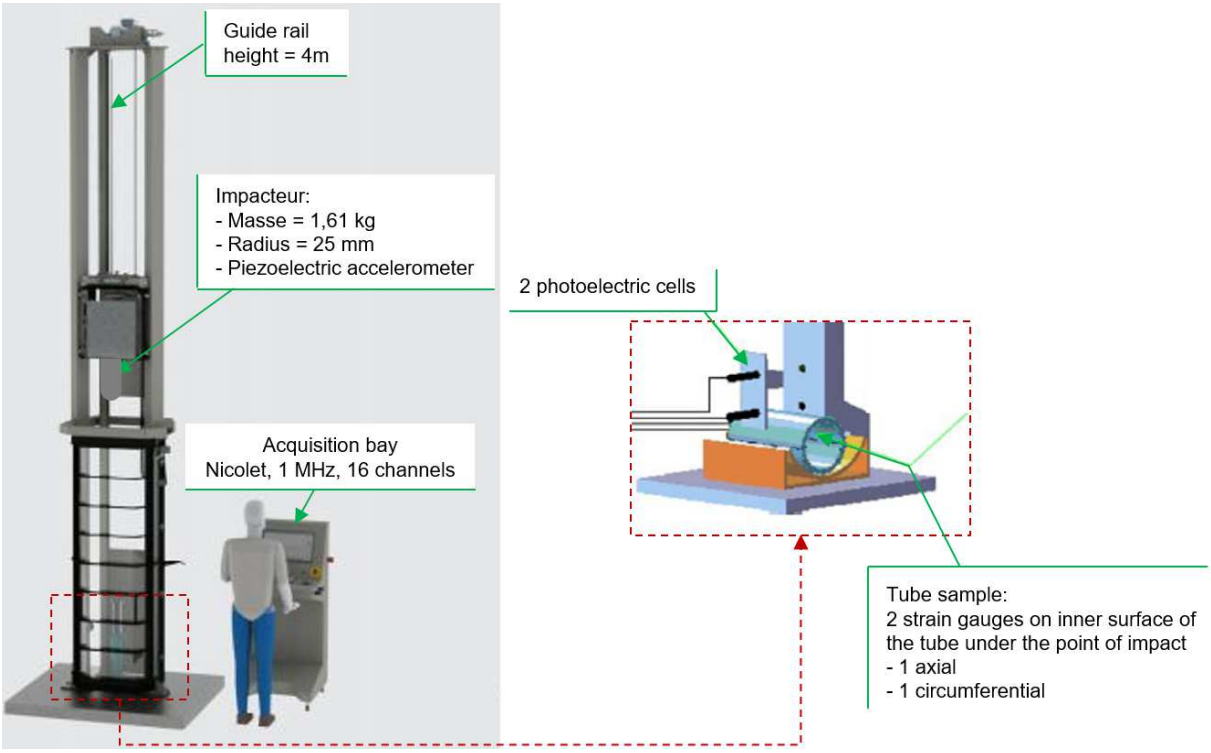

Fig. 4: Impact test setup

Following the main highlights of the experimental investigation:

- The results obtained in the impact tests are the contact force and the impactor displacement as functions of the contact time. The impact load as a function of time is proportional to the recorded acceleration signal by the impactor mass. The impactor tip displacement as a function of time is computed by double integration of the recorded acceleration signal.
- Four different impact energies are considered: 1.992 J, 5.202 J, 10.082 J and 44.760 J. Three samples for each energy level are tested. Given that the impactor mass is kept constant at 1.6 kg, the different energies level lead to analyse the effect of velocity on the dynamic response.
- Two techniques were used to quantify the damage level that occurred in the impacted samples. The first technique employed the ultrasonic C-scan to inspect the damage characterisation. The samples were placed on a rotating table into a water tank and a fixed reflector was placed in the centre of the samples. A stepper motor enables projected images of attenuation through the wall thickness to be captured. The second technique involved sectioning, polishing and microscopy tasks. Axial and longitudinal sections were realized and a fluorescent penetrant was applied to improve damage visualization. The impacted

samples were then examined and photographed under ultraviolet light. Further details of the experimental procedure are specified in [34] [35].

3.2. Finite Element Modelling

The explicit finite element software Abaqus/Explicit is used for impact simulation. Only a quarter model of the cylinder (Fig. 5) is modelled with attention to the symmetry of boundary conditions to reduce the FEA computing time. The full and quarter models were compared and a similar response was obtained [17]. The cradle which is the region of the supporting cylinder is modelled by constraining all the degrees of freedom. The impactor is defined by constraining all the degrees of freedom except for the displacement in the vertical axis to represent the experimental test conditions.

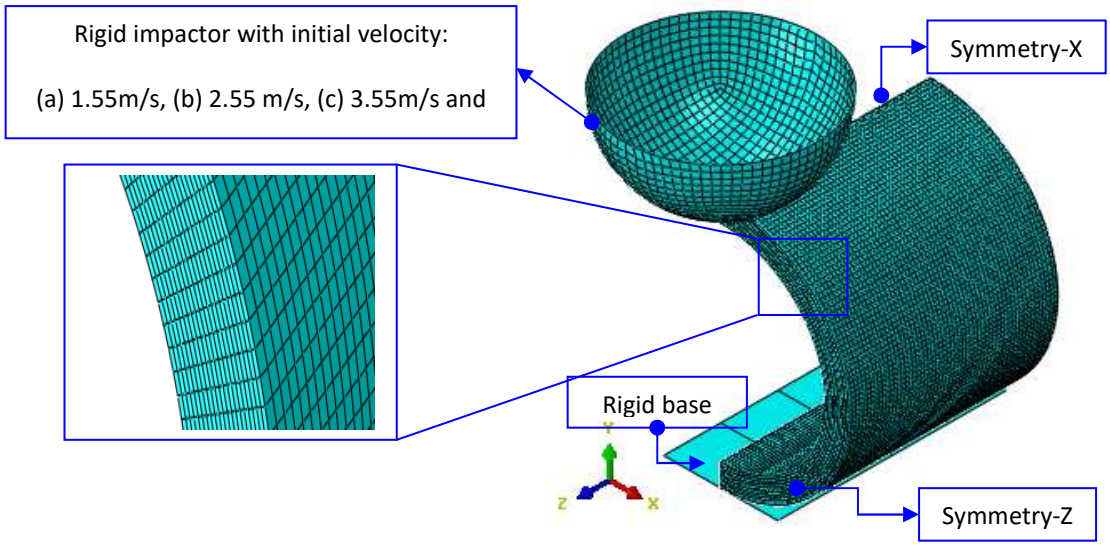

Fig. 5: Finite element quarter model for the impact analysis of the E-glass/epoxy cylinder

Total 20 plies are meshed using 8 nodes linear reduced integration solid elements (C3D8R) assigned with linear interpolation and mechanical properties listed in Fig. 4 shows the test setup employed in the experimental investigation. Materials properties including elastic and strength constants are taken from and listed in Table 2.

Table 2. A uniform smooth mesh with a single element through the thickness direction in each ply is adopted. Both the cradle and the hemispherical impactor of great stiffness compared to the cylinder are modelled as rigid bodies using R3D4 elements. Modelling cradle and impactor as deformable bodies require shell or solid elements that induce higher computation time. The impact velocity is imposed as an initial condition to the impactor's reference point.

The interaction between the impactor/cylinder and the cylinder/cradle is defined using a surface-to-surface contact algorithm based on the dynamic penalty method to avoid penetration of individual nodes of the cylinder into the rigid surfaces.

To predict the intralaminar damage of glass/epoxy cylinder under impact load, the progressive damage model is implemented as a user-defined material subroutine (VUMAT) linked with the Abaqus/Explicit. The intralaminar damage model is performed employing the different failure criteria presented in section 2. The factors s_{mT} and s_{mC} in equations 2.7, 2.8 and 2.9 are set to be equal 0.9 and 0.5 respectively [11]. Solid elements deletion from the cylinder mesh is activated. Once the element is completely damaged which means in the numerical model that the damage variable of the fibre in the tension mode reaches one, the element is deleted from the mesh to improve the computation efficiency.

3.3. Mesh Sensitivity Study

The dynamic response in terms of velocity-time and displacement-time curves of the impactor, force-time and central displacement-time curves is compared for four mesh sizes of the cylinder while the mesh size of the rigid base is remained constant 15 mm. Fig. 6 shows four mesh models including 5.0 mm x 5.0 mm, 2.0 mm x 2.0 mm, 1.0 mm x 1.0 mm and 0.5 mm x 0.5 mm which corresponds to coarse, middle, refined and extra refined mesh respectively.

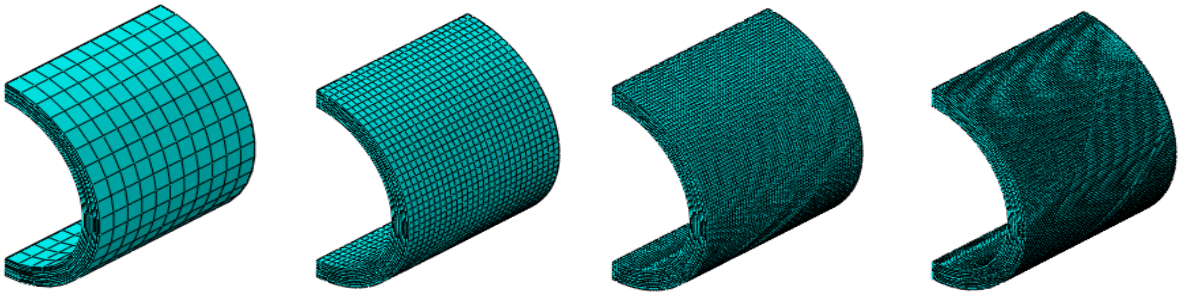

(a) Coarse mesh (5.0mm x 5.0mm) *(b) Middle mesh (2.0mm x 2.0mm)* *(c) Refined mesh (1.0mm x 1.0mm)* *(d) Extra refined mesh (0.5mm x 0.5mm)*

Fig. 6: Finite element model for the impact analysis of the composite cylinder with four mesh sizes

Fig. 7 shows the comparison of the dynamic response at 1.992 J impact energy of the four meshes. The coarse mesh presents numerical oscillations in the force-time curve and leads to a significant difference in the dynamic response in comparison with the other mesh sizes. On

the other hand, the middle mesh presents less discrepancy but the force-time curve still presents oscillations. The coarse mesh and middle mesh are therefore set aside. The refined mesh and extra refined mesh present equivalent levels and peak to peak magnitudes of the impact force.

Fig. 8 compares more specifically the impact force-time curves of the middle mesh (2.0 mm x 2.0 mm), the refined mesh (1.0 mm x 1.0 mm) and the extra refined mesh (0.5 mm x 0.5 mm) with the experimental curve denoted *"experimental Result"* at a non-damaging impact energy (1.992 J). Both mesh sizes present a similar level of stress and lead to consistent shape and magnitudes with the experimental curve. This correlation provides credibility to the FEA model as a whole. However, to ensure the accuracy of the FEA model and reduce the computation time it is not recommended to reduce the mesh size below 1.0 mm x 1.0 mm (refined mesh).

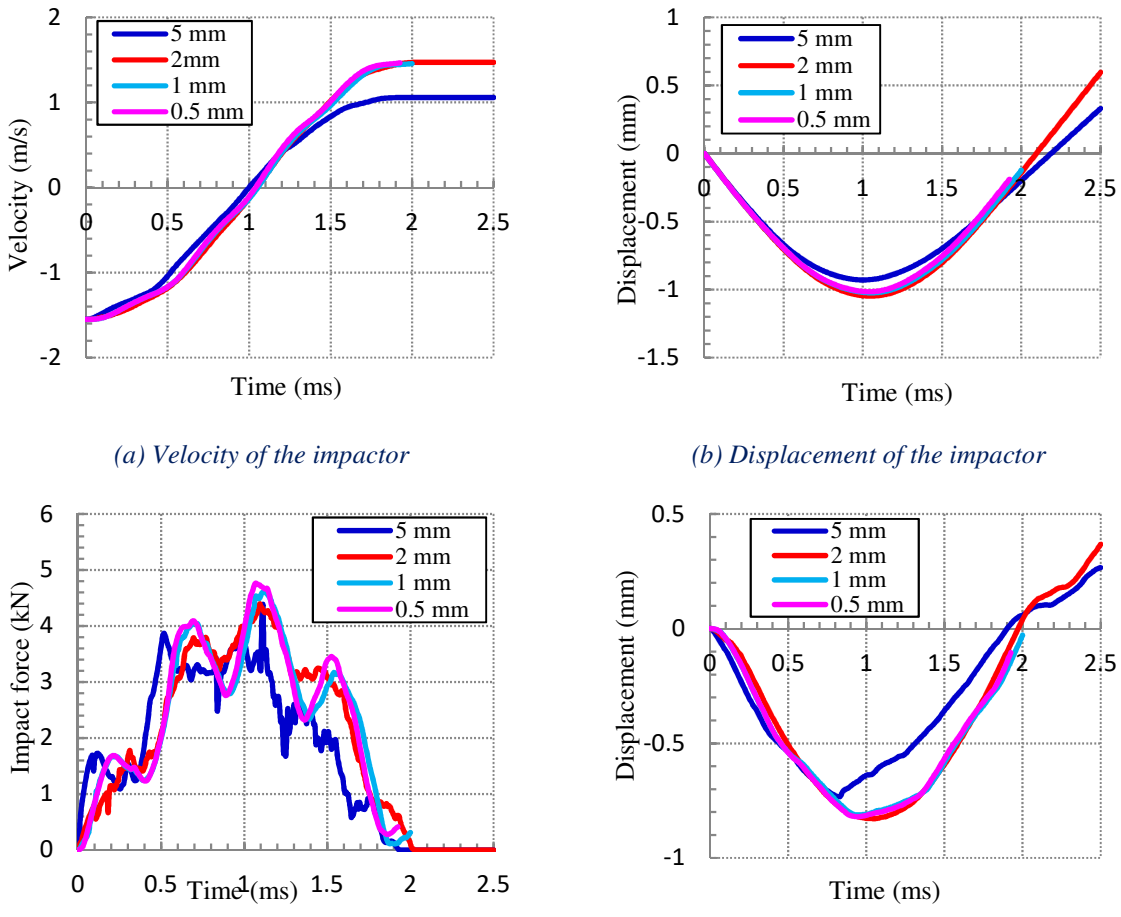

(a) Velocity of the impactor

(b) Displacement of the impactor

(d) Impact force

(c) Displacement of the central node

Fig. 7: Mesh effect on the dynamic response for non-damaging impact at 1.992 J, V=1.55 m/s

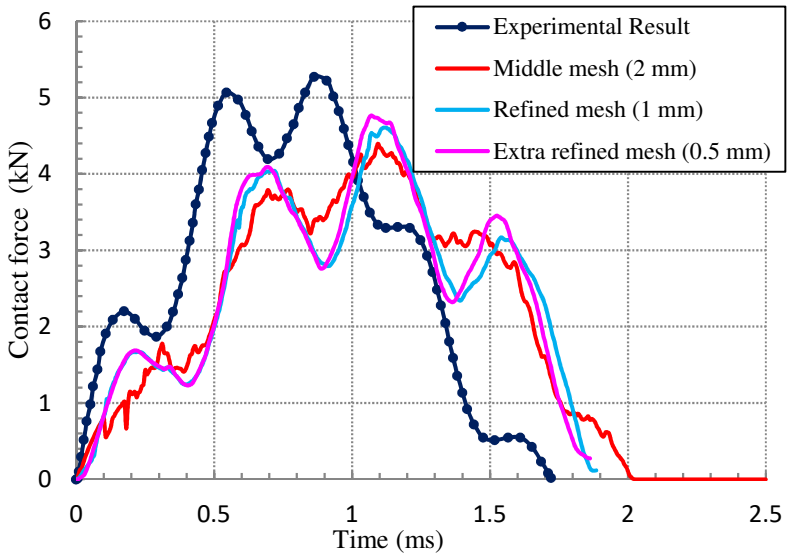

Fig. 8: Numerical and experimental impact force for non-damaging impact at 1.992 J, V=1.55 m/s

3.4. Intralaminar Damage Results

Simulations are carried out applying four failure criteria denoted *"Hashin Extend"*, *"Chang & Chang (1987)"*, *"Hashin-Puck"* and *"Hashin 3D (1980)"* which were implemented into a VUMAT subroutine linked to Abaqus/Explicit software. The bilinear model includes damage onset based on quadratic stress criteria, linear damage evolution law and element deletion from the mesh once the element is fully damaged. The intralaminar model and related equations are detailed in section 2. Three impact velocities of 2.55 m/s, 3.55 m/s and 7.48 m/s which correspond respectively to 5.202 J, 10.082 J and 44.760 J are used in the FEA model. Numerical results using FEA are compared with the impact test results published in [34] [35] in terms of force-time and displacement-time curves. At this stage interface delamination is not yet activated in the FEA model as the first objective is to assess the effect of the intralaminar failure criteria on the dynamic response.

Fig. 9 shows the force-time and displacement-time curves using four failure criteria at three impact energy levels. FEA filtering technique is used for the three impact energies to reduce oscillation in the force-time curves. In this FEA, numerical oscillation increases with impact energy due to the dynamic response of the damaged plies of the cylinder. By comparing with experimental results, numerical results denoted *"Hashin Extend"* and *"Chang & Chang (1987)"* show lower precision than those denoted *"Hashin-Puck"* and *"Hashin 3D (1980)"* where the force-time curves are smooth and present a well-predicted shape. *"Hashin Extend"* and *"Chang & Chang"* criteria considerably overestimate both the maximum displacement of

the impactor and the rebound process until the complete separation between the impactor and the cylinder but *"Hashin 3D (1980)"* and *"Hashin-Puck"* lead to closer results. A relatively acceptable agreement of the force-time curve is obtained between experimental results and numerical results denoted *"Hashin 3D (1980)"* and *"Hashin-Puck"* criteria at 5.202 J and 10.082 J impact energies. At 44.760 J impact energy, the force-time curve of both *"Hashin 3D (1980)"* and *"Hashin-Puck"* criteria shows lower accuracy compared to experimental results and significantly more numerical oscillation appears which indicates the occurrence of severe damage. Both the predicted contact time and the impactor displacement are longer at 44.760 J impact energy compared with the experimental curves because the cylinder develops more damage. By comparison with experimental results, the first damage load obtained by FEA is relatively well captured at 5.202 J and 10.082 J impact energies except for the *"Hashin Extend"* criteria where the FEA model presents inaccurate magnitudes. Extending two-dimensional quadratic failure criteria to the three-dimensional case through the addition of the out-of-plane stress components as carried out in the *"Hashin Extend"* FEA model would not necessarily provide 3D failure criteria even with quadratic stress interaction between failure modes. This statement leads to excluding the criteria denoted *"Hashin Extend"* from the FEA comparison. At 5.202 J impact energy the values of the first damage load by *"Hashin 3D (1980)"*, *"Hashin-Puck"*, *"Chang & Chang (1987)"* criteria and experiments are about 3.047 kN, 2.874 kN, 2.693 kN and 3.896 kN respectively, and at 10.082 J impact energy about 4.311 kN, 3.769 kN, 3.718 kN and 5.387 kN respectively. The figures show that the predicted first load damage is lower than the experimental values. Beyond the first damage time, the predicted impact force is strongly affected by the failure criteria used in the FEA. By comparison with experimental data [34] [35], *"Chang & Chang (1987)"* criteria lead to larger errors. Putting aside *"Chang & Chang (1987)"* criteria, *"Hashin 3D (1980)"* criteria lead to higher precision and well description of the force-time curve than *"Hashin-Puck"* criteria in which the transverse compression mode is based on the Puck failure theory. However, Puck theory [36] is considered as an improvement of the Hashin theory [19] as more detailed considerations of the 3D failure mechanism are figured out and particularly the fracture angle due to the transverse compression load. The possible reason is that the fracture plane angle as oriented in the *"Hashin-Puck"* FEA model might not be suitable for the shear failure of filament-wounded cylindrical structures. Basically, the fracture angle was determined for uniaxial transverse compressive load case rather than impact. Hence, an accurate determination of the fracture plane angle in the case of wounded cylinders under impact loads would be an interesting investigation.

Fig. 10 shows the matrix tension damage and matrix compression damage of the cylinder using *"Hashin 3D (1980)"* failure criteria at the complete separation between the impactor and the cylinder. Two damage variables called SDV3 and SDV4 in the VUMAT code are defined for matrix tension damage and matrix compression damage respectively. The damage of the matrix in both tension and compression becomes more severe with the increase in impact energy. Matrix tension is found to be the dominant damage mode compared with matrix compression damage in the range of impact energies. The predicted matrix damage is well concentrated around the impact region and presents a pyramidal shape. Nevertheless, a little evidence of fibre breakage is obtained in the area in contact with the impactor. The predicted pyramidal damage is consistent in terms of damage shape with the experimental observation of Gning et al. [34] [35]. The test results showed that beyond 4J impact energy, transverse intra-layer cracks and delamination appear and extend more significantly with the increase of impact energy. The transverse cracks and delamination propagate through the cylinder thickness in a pyramidal shape of damage volume (Fig. 11). This phenomenon is similar to what is reported in the case of impact on flat panels [37]. Gning et al. [34] [35] have shown that the damage extends further along the tube axis than around the circumference. As a whole result, the progressive damage model implemented into the VUMAT subroutine using *"Hashin 3D (1980)"* failure criteria is considered as a relatively good compromise between the model accuracy and the computing time in the range of 5 J and 10 J but on another hand, the damage model still requires the consideration of the effect of delamination. Therefore the purpose of the section 3.4 is to include the delamination effect in the numerical modelling.

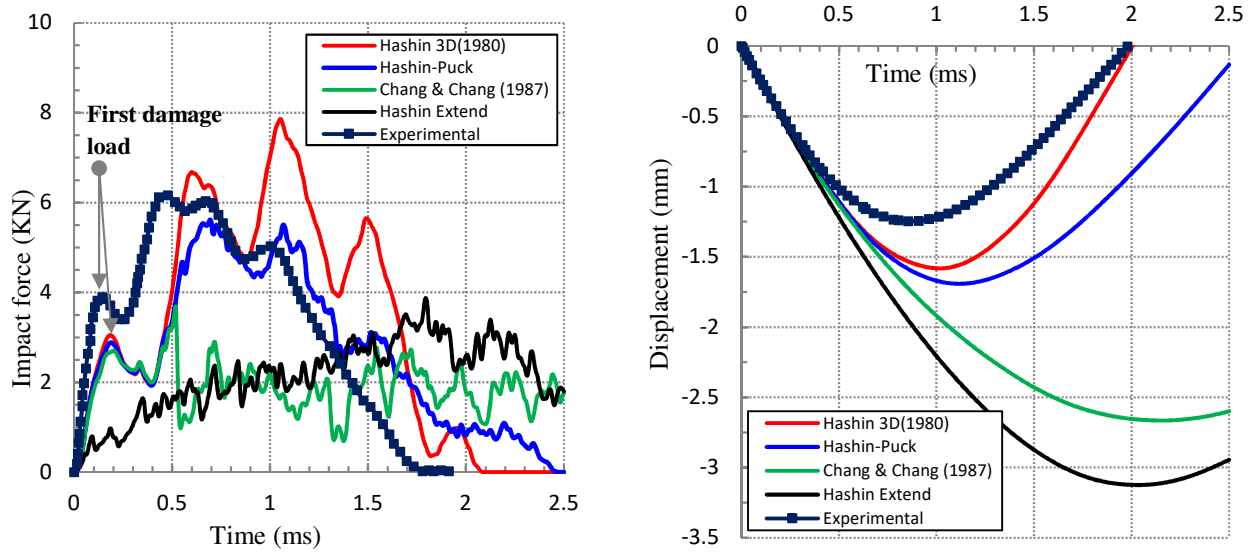

(a) Impact energy 5.202 J (V=2.55 m/s)

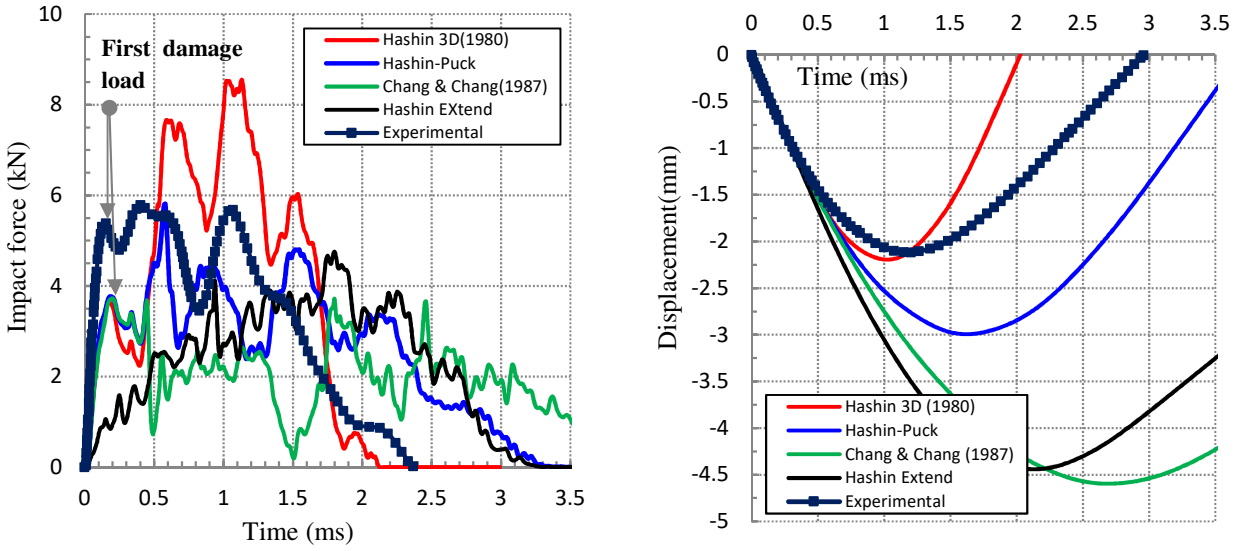

(b) Impact energy of 10.082 J (V=3.55 m/s)

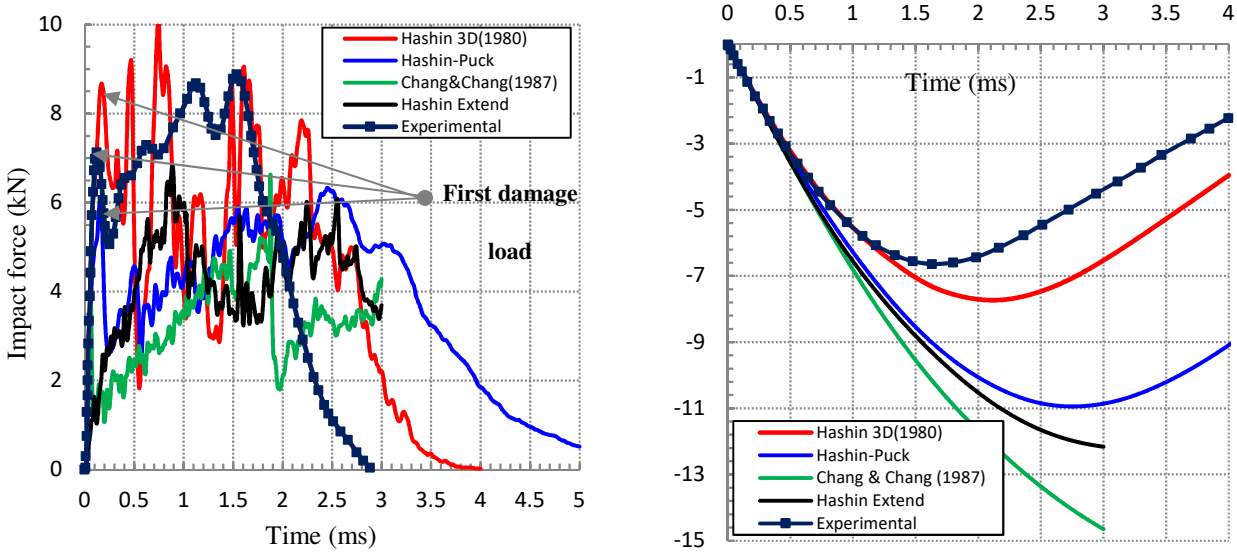

(c) Impact energy of 44.760 J (V=7.48 m/s)

Fig. 9: Numerical and experimental force-time and displacement-time comparison using various intra-laminar failure criteria for different impact energies

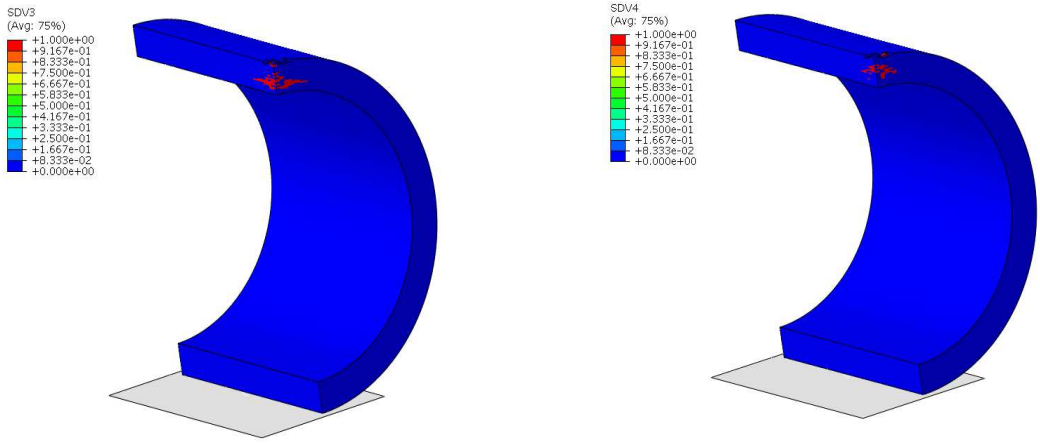

Matrix tension mode *Matrix compression mode*

(a) Impact of 5.202 Joules (V=2.55 m/s)

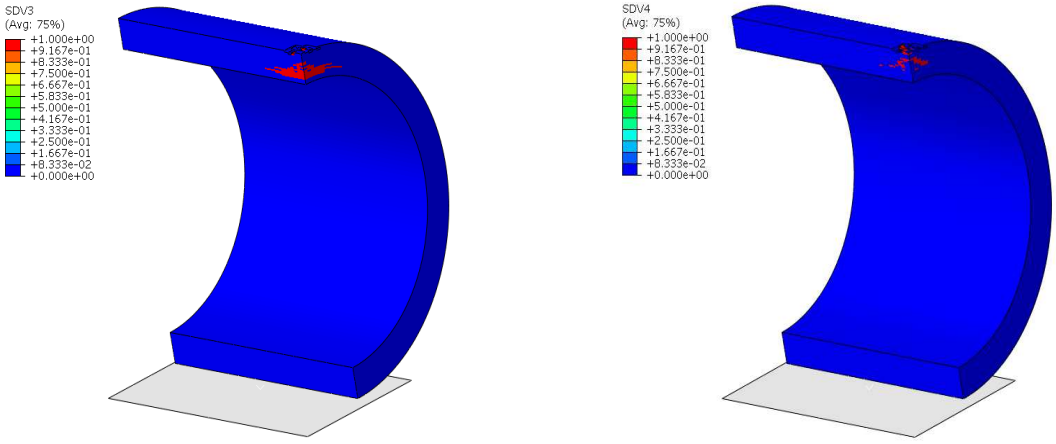

Matrix tension mode *Matrix compression mode*

(b) Impact energy of 10.082 Joules (V=3.55 m/s)

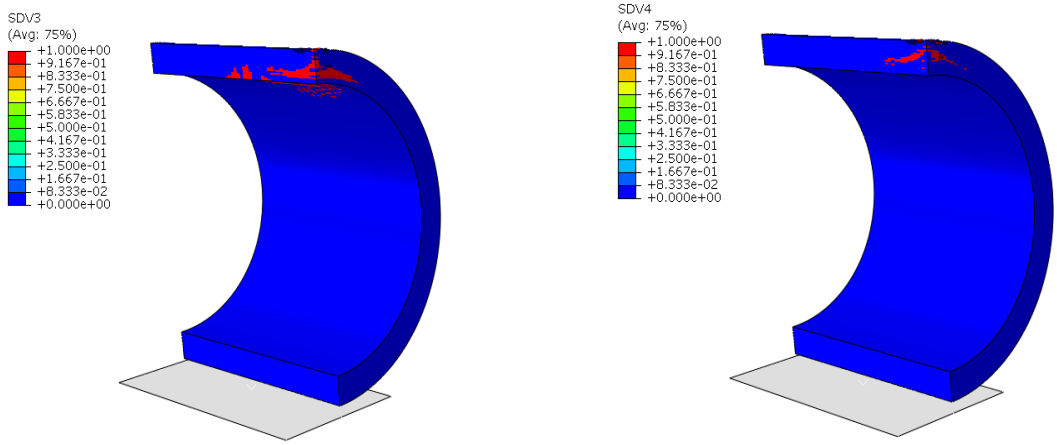

Matrix tension mode *Matrix compression mode*

(c) Impact energy of 44.76 Joules (V=7.48 m/s)

Fig. 10: Prediction of the through-thickness matrix tension damage and matrix compression damage using *"Hashin 3D (1980)"* failure criteria for three impact energies at the end of the impact analysis

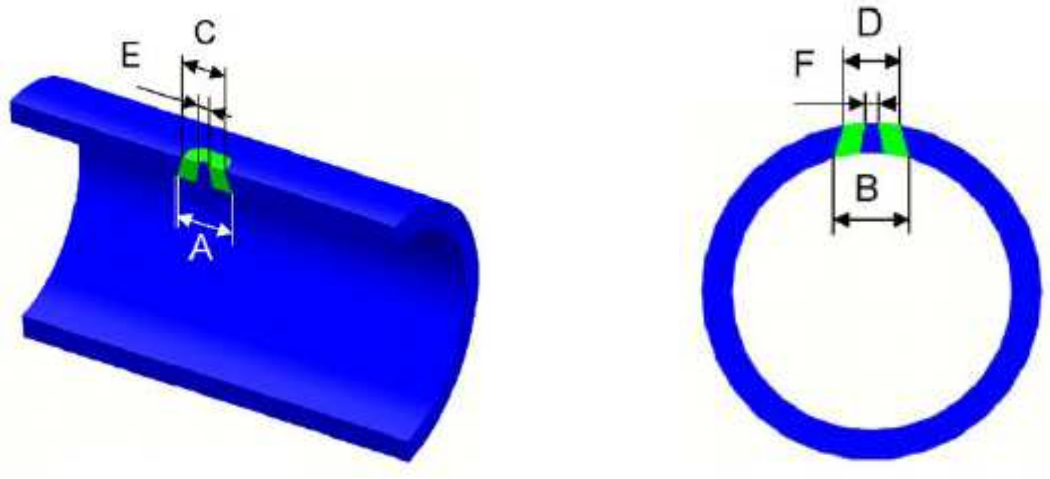

(a) Axial dimensions *(b) Circumferential dimensions*

Fig. 11: Schematic diagram showing measured dimensions in impacted damage area

3.4. Interlaminar damage combination

The experimental observation of Gning et al. [34] [35] pointed out also the occurrence of delamination between plies promoted through the thickness intralaminar matrix cracks. However, the intralaminar damage model implemented into the VUMAT subroutine using "*Hashin 3D (1980)"* criteria requires improvement and it is necessary to consider the influence of interface delamination on the predicted progressive damage. The combination of the interlaminar damage model with the intralaminar damage model leads to enhance the predicted progressive damage but a higher computation time and modelling complexity are required.

Interlaminar delamination is now combined with the "*Hashin 3D (1980)"* FEA model through interface interaction based on the cohesive zone theory. This approach leads to combine the ply failure described in the intralaminar constitutive model with the cohesive zone model (CZM) and the interaction between both damage models as well. A cohesive contact is applied to the surface nodes between all layers of the cylinder. A total of 19 interfaces were modelled as a cohesive contact and the bilinear traction-separation law available in Abaqus/Explicit was employed. The initial response of the cohesive contact is assumed to be linear and the damage is initiated once the stress failure function is satisfied. Camanho et al. [38] show poor results when the maximum stress criterion is used and suggest the quadratic failure stress function as:

$$\left(\frac{\sigma_n}{N}\right)^2 + \left(\frac{\sigma_s}{S}\right)^2 + \left(\frac{\sigma_t}{T}\right)^2 \geq 1 \qquad (24)$$

Where σ_n, σ_s and σ_t denote the traction stress vector in the normal (n) and shear directions t and s respectively. N, S and T are the interlaminar normal and two shear strengths respectively.

Once the delamination initiation reaches 1 (equation (24) = 1), the delamination propagation is modelled as a degradation of the interface stiffness following a linear softening law, Fig. 12. Similar to the intralaminar damage model, a scalar damage variable (d) is defined to represent the delamination propagation under mixed-mode loading [38].

$$d = \frac{\delta_m^f(\delta_m^{Max} - \delta_m^0)}{\delta_m^{Max}\left(\delta_m^f - \delta_m^0\right)} \left\{ \begin{array}{l} \delta_m = \sqrt{(\delta_1^2 + \delta_2^2 + \langle\delta_3\rangle^2)} \\ \delta_m^{Max} = max(\delta_m^{Max}, \delta_m) \\ \delta_m^0 = \delta_3^0\delta_1^0\sqrt{\frac{1+\beta^2}{(\delta_1^0)^2+(\beta\delta_3^0)^2}}, (\delta_3 > 0) \\ \delta_m^0 = \sqrt{(\delta_1^0)^2 + (\delta_2^0)^2}, (\delta_3 \le 0) \\ \delta_1^0 = S/K_s, \delta_2^0 = T/K_t, \delta_3^0 = N/K_n, \beta = \left(\sqrt{\delta_1 + \delta_2}\right)/\delta_3 \\ \delta_m^f = \frac{2}{k\delta_m^0}\left[G_I^c + (G_{II}^c - G_I^c)\left(\frac{\beta^2}{1+\beta^2}\right)^n\right], (\delta_3 > 0) \\ \delta_m^f = \sqrt{\left(\delta_1^f\right)^2 + \left(\delta_2^f\right)^2}, (\delta_3 \le 0) \\ i=1,2 \text{ (mode II, III)} \\ i=3 \text{ (mode I)} \end{array} \right. \quad (25)$$

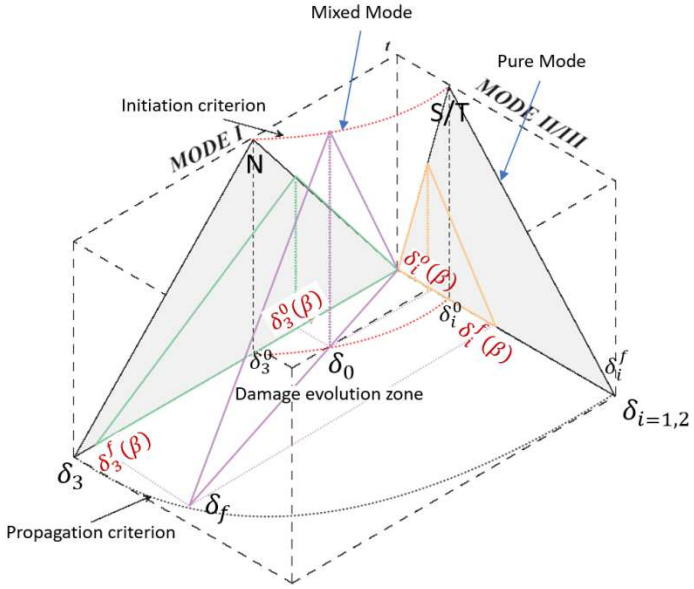

Fig. 12: Mixed Mode softening law behaviour

The damage variable (d) varies from 0 when the interface delamination is initiated to 1 at the complete delamination of the interface. δ_m, δ_m^0, $\delta_m^f$and δ_m^{Max} represent the mixed-mode displacement, the mixed-mode onset displacement, the mixed-mode final displacement at the complete interface decohesion and the mixed-mode maximum displacement respectively. δ_1^0, δ_2^0, δ_3^0 represent the single-mode onset displacement. β is the mixity mode ratio. K_n, K_s and K_t are the interfacial penalty stiffness. G_I^c, G_{II}^c and G_{III}^c are the critical interlaminar fracture toughness in Mode I, II and III respectively. The Benzeggagh-Kenane criterion (B-K criterion) based on fracture energy is used to predict the delamination propagation under mixed-mode loading. The critical energy release rate (G_c) is given as:

$$G_c = G_I^c + \left(G_{II}^c - G_{III}^c\right)\left(\frac{G_{II} + G_{III}}{G_T}\right)^n \qquad (26)$$

$$G_T = G_I + G_{II} + G_{III}$$

G_T is the total energy release rate and n is a material parameter obtained from the mixed-mode bending test [38]. The mathematical formulation of the CZM and related parameters of the irreversible mixed-mode softening law are well described in the NASA report [39].

The properties required in the interlaminar model are listed in Table 3. The interfacial penalty stiffness is set to be high values (k=10E8) as recommended by Camanho et al. [38]. n =1 is adopted in the FEA model. Gning et al. [34] [35] did not carry out standardized tests such as DCB (double cantilever beam), ENF (end notched flexure) and MMB (mixed mode bending) to obtain the critical fracture toughness. The interface properties are taken from Menna et al.

[40] for a similar E-glass epoxy unidirectional composite. The *"Hashin 3D (1980)"* failure criteria implemented into the Vumat subroutine is now combined with the interface model based on the cohesive theory through an uncoupled approach.

Table 3: Properties used in the cohesive model [40]

$K_n = K_s = K_t$ (N/mm^3)	N (MPa)	T (MPa)	S (MPa)	G_{Ic} (N/mm)	$G_{IIc} = G_{IIIc}$ (N/mm)	Power factor of the B-K criterion
10E8	35	65	65	0.345	0.6	1

Fig. 13 shows the force-time and displacement-time curves using intralaminar and interlaminar model combination denoted *"Vumat-CZM"* compared with the experimental data denoted *"Experimental"* at two impact energies level of 5.202 J and 10.082 J which correspond respectively to 2.55 m/s and 3.55 m/s impact velocities. The combination of the intralaminar damage model with the interface model required smaller stable time increments and a larger amount of increments to complete the simulation time (roughly 2.5 ms). This is mainly due to the considerable number of composite plies combined with cohesive interfaces. The filtering technique used earlier in the intralaminar model was maintained but the whole shape of the impact force presents more oscillations. This behaviour can be caused by the matrix cracks combined with interface delamination. It is clear from Fig. 13 that the predicted dynamic response in terms of impact force and impactor displacement for both impact energies is improved when delamination is considered in the FEA model but heavy simulation and higher computing time are required.

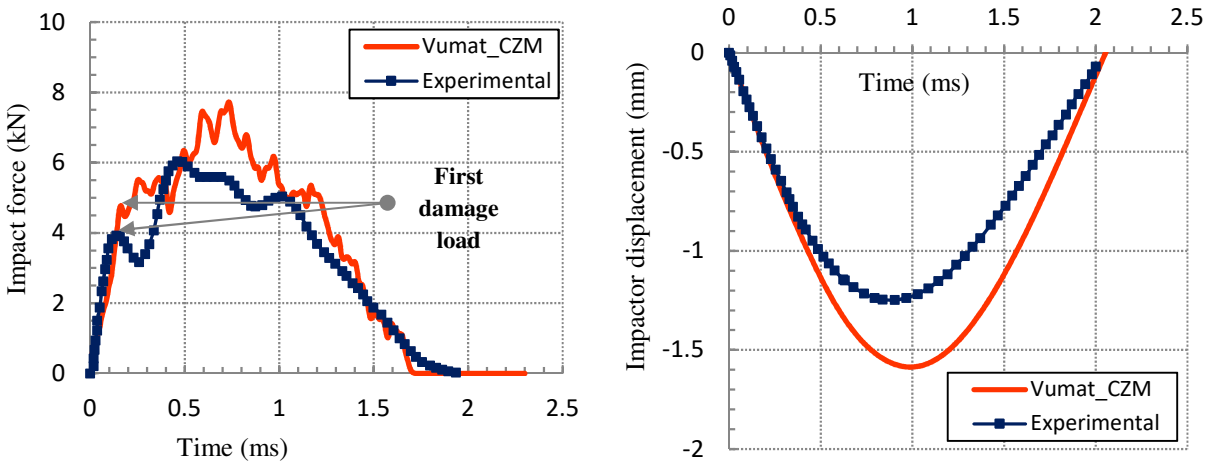

(a) Impact energy 5.202 J (V=2.55 m/s)

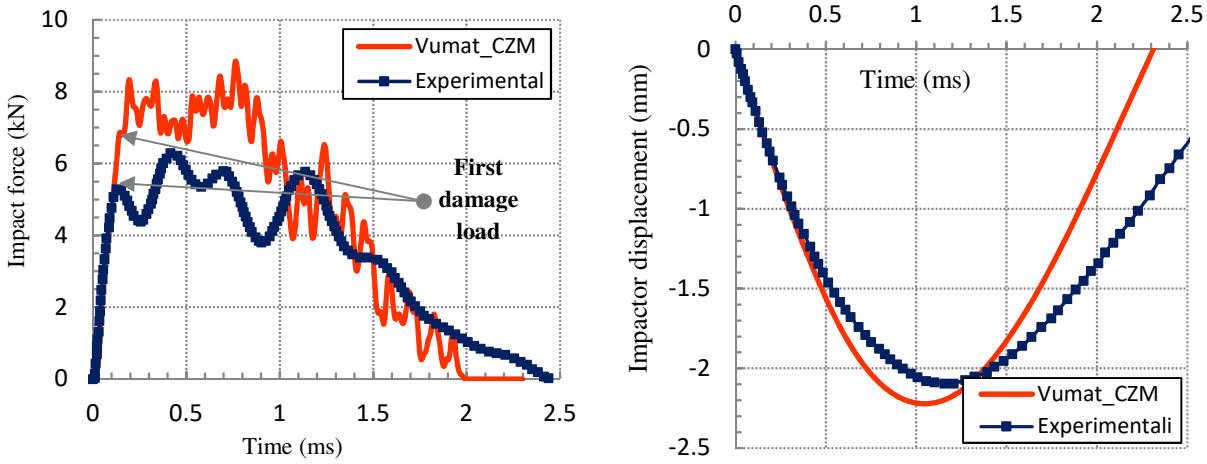

(b) Impact energy of 10.082 J (V=3.55 m/s)

Fig. 13: Numerical and experimental force-time and displacement-time comparison using intralaminar and interlaminar damage combination for different impact energies

The values of the first damage load by *"Vumat-CZM"* and experimental results *"Experimental"* at 5.202 J impact energy are about 4.718 kN and 3.896 kN respectively, and at 10.082 J impact energy about 6.680 kN and 5.387 kN respectively. The figures show that the predicted first load damage is higher than the experimental value when the delamination model is included in the simulation but reasonable magnitudes are obtained. Fig. 13 shows overestimation of load peaks even if the delamination model is combined with the intralaminar model. This result can be related to the fracture energies which may present incertitude and can affect the dynamic response. It should be mentioned that in the present cohesive model the interface properties were taken from a similar E-glass-epoxy material. If

the measured properties are used to feed the cohesive model the accuracy of the predicted dynamic response is intended to be improved. Nevertheless, the FEA model based on intralaminar and interlaminar damage combination by employing an uncoupled approach has demonstrated its usefulness for the prediction of the dynamic response.

4.4. Influence of interface properties

Interface properties used as inputs in the cohesive damage model are challenging to obtain experimentally and errors made in the experimental measurement of interfacial strengths and critical fracture toughness affect the delamination onset and propagation. Therefore the influence of the variation of interface properties on the dynamic response is analyzed. A reverse calculation that uses the interface properties taken from the literature [40] as a baseline is employed to discuss the sensitivity of the cohesive model at 5.202 J and 10.082 J impact energies. The influence of interface properties is carried out by varying interfacial strengths as shown in Table 4 while the critical fractures toughness are maintained constant such as described in the baseline model. The critical fractures toughness are then varied as shown in Table 5 while the interfacial strengths are maintained constant such as described in the baseline model. Interface properties including interfacial strengths and critical fractures toughness are varied to be lower and higher from the baseline FEA model while keeping the interfacial penalty stiffness and the parameter *n* constants.

Table 4: Variation of the interface strengths values ($\boldsymbol{K_n = K_s = K_t = 10E8}$)

	$\boldsymbol{N}$ *(MPa)*	$\boldsymbol{T = S}$ *(MPa)*	**Power factor of the B-K criterion**
Case A	30	55	1
Baseline	35	65	1
Case B	45	75	1

Table 5: Variation of critical fracture toughness values ($\boldsymbol{K_n = K_s = K_t = 10E8}$)

	$\boldsymbol{G_{Ic}}$ $(\boldsymbol{N/mm})$	$\boldsymbol{G_{IIc} = G_{IIIc}}$ $(\boldsymbol{N/mm})$	**Power factor of the B-K criterion**
Case C	0.145	0.2	1
Baseline	0.345	0.6	1
Case D	0.745	1	1

Fig. 14 and Fig. 15 show the comparison between the experimental and the numerical predictions of the force-time curve using a variation of the interface strengths and the critical fracture toughness values respectively. It can be observed that the numerical impact force curve is affected by the interface properties used in the cohesive model. Also, the impact time becomes longer when the interface properties decreased. However, the global shape of the predicted force-time curve remains consistent but shifted top or bottom in comparison with the baseline curve. This is explained by the fact that the damage onset and propagation are stimulated when the interface properties are lower than the baseline model. By comparison with the experimental curve, interface strengths in case A (N=30 MPa, S=T=55 MPa) and critical fracture toughness in case C (G_I^c=0.145 N/mm, G_{II}^c=G_{III}^c=0.2 N/mm) lead to higher precision of the FEA model and therefore are expected to be the nearest to the real interface properties.

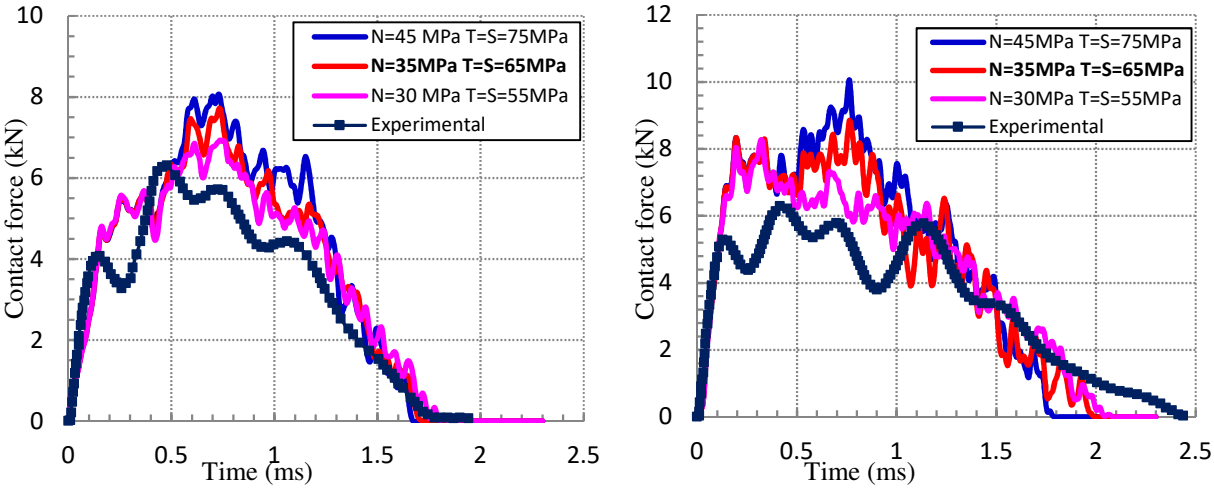

(a) Impact energy 5.202 Joules (V=2.55 m/s) *(b) Impact Energy 10.082 Joules (V=3.55 m/s)*

Fig. 14: Influence of the interlaminar strengths on the impact force curve

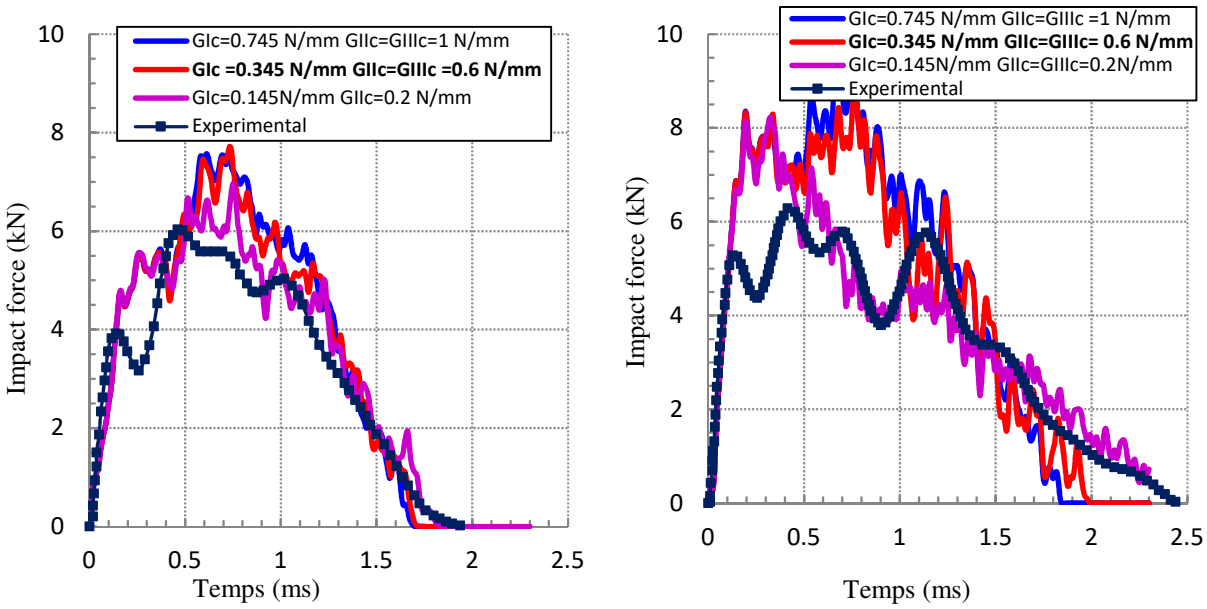

(a) Impact energy 5.202 Joules (V=2.55 m/s) *(b) Impact Energy 10.082 Joules (V=3.55 m/s)*

Fig. 15: Influence of the critical fractures toughness on the impact force curve

5. Conclusion

The dynamic progressive damage behaviour of thick glass epoxy cylindrical structure subjected to low-velocity impact was investigated in this paper. A progressive damage model that combines the intralaminar damage with the interlaminar delamination was developed according to the framework conditions of continuum damage mechanics. The intralaminar damage models using four failure criteria based on quadratic stress interaction and solid discretization of elements were implemented using VUMAT subroutines linked to Abaqus Explicit. The delamination is simulated by the cohesive model available in Abaqus Explicit.

The comparison between numerical and experimental results at different impact energies shows that the intralaminar damage model using “Hashin 3D (1980)” criteria presents the lowest errors while “Hashin Extend” criteria present the largest errors of the impact force and impactor displacements. The main explication is that extending two-dimensional failure criteria to the three-dimensional case by adding only the out-of-plane stress and strength components as carried out in the “Hashin Extend” FEA model does not provide three-dimensional failure criteria even with keeping a quadratic interaction between failure modes.

“Hashin 3D (1980)” failure criteria is considered as a relatively good compromise between the model accuracy and the computing time but not entirely sufficient to describe the full damage mechanism as it is essential to combine the intralaminar model with the delamination

model for a better prediction of the dynamic response. The intralaminar and interlaminar models combination is based on an uncoupled approach. The numerical results are of the same order of magnitude as the experimental measurements but heavy simulation and higher computing time are required. The interlaminar model is sensitive to interface properties used to feed the cohesive law. Interface properties affect the delamination onset and propagation when errors are made in the measurement of interfacial strengths and critical fracture toughness. The reverse calculation allowed estimating numerically the effective interface properties using experimental results and a baseline FEA model. The modelling approach has proven to be capable of reproducing experimental results with acceptable accuracy. The damage model developed in this paper presents a baseline for our future investigation in terms of damage prediction and failure mechanism in filament wounded cylindrical structures under impact loads. Finally, the modelling methodology is intended to be applied in the design loop and development of the MJM tidal turbine concept where thick filament wound glass/epoxy cylinders are used in the design investigation to carry dynamic loads.

Acknowledgment

The authors would like to thank BMO "Brest Métropole Océane" for their financial support of this Ph.D project.

References

[1] D. M. Grogan, S. B. Leen, C. R. Kennedy and C. M. Ó Brádaigh, "The Advances of Composite Material in Marine Renewable Energy Structures," *Renewable Energy,* vol. 57, pp. 151-162, 2013.

[2] M. Ait Mohammed, M. Tarfaoui and J.-M. Laurens, "Composite Tidal Turbine: Compromise between hydrodynamic efficiency and impact damage safety," in *24th CFM*, Brest, 26-30 August 2019, France, 2019.

[3] M. Ait Mohammed, "Study of Composites Ducts for Optimal Design of an Horizontal Axis Tidal Turbine," PhD Thesis, ENSTA Bretagne, 2017.

[4] M. L. Kachanov, On The Time to Failure Under Creep Conditions, Izv. AN SSSR, 1958.

[5] J. Lemaitre and J. L. Chaboche, Mechanics of Solid Materials, Cambridge University Press, 1990.

[6] J. Maire and J. Chaboche, "A new formulation of continuum damage mechanics (CDM) for composite materials," *Aerospace Science and Technology,* vol. 4, pp. 247-257, 1997.

[7] P. Ladevèze, O. Allix, J. F. Deü and D. Lévêque, "A mesomodel for localisation and damage computation in laminates," *Computer Methods in Applied Mechanics and Engineering,* vol. 183, pp. 105-122, 2000.

[8] H. Singh, K. K. Namala and P. Mahajan, "A damage evolution study of E-glass/epoxy composite under low velocity impact," *Composites Part B,* vol. 76, pp. 235-248, 2015.

[9] P. F. Liu, B. B. Liao and X. Q. Peng, "Finite element analysis of dynamic profressive failure of carbon fiber composite laminates under low velocity impact," *Composite Structures,* vol. 149, pp. 408-422, 2016.

[10] W. He, Z. Guan, X. Li and D. Liu, "Prediction of permanent indentation due to impact on laminated composites based on an elasto-plastic model incorporating fiber failure," *Composite Structures,* vol. 96, pp. 232-242, 2013.

[11] B. B. Liao and P. F. Liu, "Finite element analysis of dynamic progressive failure of plastic composite laminates under low velocity impact," *Composite Structure,* vol. 159, pp. 567-578, 2017.

[12] P. F. Liu, B. B. Liao, L. Y. Jia and X. Q. Peng, "Finite element analysis of dynamic progressive failure of carbo fibre composite laminates under low velocity impact," *Composite Structures,* vol. 149, pp. 408-422, 2016.

[13] K. Krishnamurthy, P. Mahajan and R. Mittal, "Impact Response and Damage in Laminated Composite Cylindrical Shells," *Composite Structures,* vol. 59, pp. 15-36, 2003.

[14] S. M. R. Khalili, M. Soroush, A. Davar and O. Rahmani, “Finite element modeling of low-velocity impact on laminated composite plates and cylindrical shells,” *Composite Structures,* vol. 93, p. 1363–1375, 2011.

[15] I. Hyeon Choi, “Low-velocity impact response analysis of composite pressure vessel considering stiffness change due to cylinder stress,” *Composite Structures,* vol. 160, p. 491–502, 2017.

[16] M. Tarfaoui and P. B. Gning, “Experimental Investigation and Finite Element Analysis of Dynamic Behavior and Damage of Glass/Epoxy Tubular Structures,” *Key Engineering Materials,* Vols. 471-472, pp. 951-956, 2011.

[17] M. Tarfaoui, P. B. Gning and L. Hamitouche, “Dynamic response and damage modeling of glass/epoxy tubular structures: Numerical investigation,” *Composites Part A: applied science and manufacturing,* vol. 39, pp. 1-12, 2008.

[18] Z. Hashin and A. Rotem, “A Fatigue Failure Criterion for Fiber Reinforced Materials,” *Composite Materials,* vol. 7, pp. 448-464, 1973.

[19] Z. Hashin, “Fatigue Failure Criteria for Unidirectional Fiber Composite,” DEPARTMENT OF MATERIALS SCIENCE AND ENGINEERING , UNIVERSITY OF PENNSYLVANIA, 1980.

[20] F. Chang and K. Chang, “A progressive damage model for laminated composite containing stress concentrations,” *Journal of composite Materials,* vol. 21, p. 834–855, 1987.

[21] A. Puck and H. Schurmannb, “Failure analysis of FRP laminates by means of physically based phenomenological models,” *Composites Science and Technology,* vol. 62, p. 1633–1662, 2002.

[22] G. Alfano and M. A. Crisfield, “Finite Element Interface Models for the Delamination Analysis of Laminated Composites: Mechanical and Computational Issues,” *International Journal for Numerical methods in Engineering,* vol. 50, pp. 1701-1736, 2001.

[23] W. Guo, P. Xue and J. Yang, “Nonlinear progressive damage model for composite laminates used for low-velocity impact,” *Applied Mathematics and Mechanics,* vol. 34, p. 1145–1154, 2013.

[24] J. Pederson, “Finite Element Analysis of Carbon Fiber Composite Ripping Using ABAQUS,” Master of Science (MS), Clemson University, 2008.

[25] F. París, “A Study of Failure Criteria of Fibrous Composite Materials,” Langley Research Center, 2001.

[26] M. Meo, A. Morris, R. Vignjevic and G. Marengo, “Numerical simulations of low-velocity impact on an aircraft sandwich panel,” *Composite Structures,* vol. 62, p. 353–360 , 2003.

[27] G. Lutz, “The Puck theory of failure in laminates in the context of the new guideline VDI 2014 Part 3,” in *Proceedings of a Conference on Damage in Composite Materials 2006*, Stuttgart, Germany., 2006.

[28] M. Deuschle, “3D Failure Analysis of UD Fibre Reinforced Composites: Puck’s Theory within FEA,” PhD Thesis. Institute of Statics and Dynamics of Aerospace Structures. University of Stuttgart, 2010.

[29] I. Lapczyk and J. A. Hurtado, “Progressive damage modeling in fiber-reinforced materials,” *COMPOSITES Part A: Applied science and manufacturing,* vol. 38, pp. 2333-2341, 2007.

[30] S. H. Xin and H. M. Wen, “A progressive damage model for fiber reinforced plastic composites subjected to impact loading,” *International Journal of Impact Engineering,* vol. 75, p. 40–52, 2015.

[31] Z. Bažant and B. Oh, “Crack band theory for fracture of concrete,” *Materials and Structures,* vol. 16, pp. 155-177, 1983.

[32] Z. Bažant and G. Pijaudier-Cabot, “Nonlocal Continuum Damage Localization, Instability and Convergence,” *Journal of Applied Mechanics,* vol. 55, pp. 287-293, 1988.

[33] G. Pijaudier-Cabot and L. Bode, “Localization of damage in a nonlocal continuum,” *Mechanics Research Communications,* vol. 19, pp. 145-153, 1992.

[34] P. B. Gning, M. Tarfaoui, F. Collombet and P. Davies, “Damage development in thick composite tubes under impact loading and influence on implosion pressure : Experimental observations,” *Composites Part B: engineering,* vol. 36, pp. 306-318, 2005.

[35] P. B. Gning, M. Tarfaoui, F. Collombet and P. Davies, “Prediction of damage in composite cylinders after impact,” *Journal of Composite Materials,* vol. 39, pp. 17-28, 2005.

[36] A. Puck and H. Schürmann, “Failure Analysis of FRP Laminates by Means of Physical Based Phenomenological Model,” *Composites Science and Technology,* vol. 58, p. 1045–1067, 1998.

[37] L. S. Kistler and A. M. Waas, “On the response of curved laminated panels subjected to transverse impact loads,” *International Journal of Solids and Structures,* vol. 36, pp. 1311-1327, 1999.

[38] P. P. Camanho, C. G. Davila M and M. F. de Moura, “Numerical Simulation of Mixed-Mode Progressive Delamination in Composite Materials,” *Journal of Composite Materials,* vol. 37, pp. 1415-1438, 2003.

[39] P. P. Camanho and C. G. Dàvilla, “Mixed-Mode decohesion finite elements for the simulation of delamination in composite materials,” Tech Rep NASA/TM2002-211737, 2002.

[40] C. Menna, D. Asprone, G. Caprino, V. Lopresto and A. Prota, “Numerical simulation of impact tests on GFRP composite laminates,” *Internation Journal of Impact Engineering,* pp. 677-685, 2011.